

Pure spin current in a two-dimensional topological insulator

Xing-Tao An,^{1,2,*} Yan-Yang Zhang,¹ Jian-Jun Liu,³ and Shu-Shen Li¹

¹*SKLSM, Institute of Semiconductors, Chinese Academy of Sciences, P. O. Box 912, Beijing 100083, China*

²*School of Sciences, Hebei University of Science and Technology, Shijiazhuang, Hebei 050018, China*

³*Physics Department, Shijiazhuang University, Shijiazhuang 050035, China*

(Dated: March 1, 2013)

We predict a mechanism to generate a pure spin current in a two-dimensional topological insulator. As the magnetic impurities exist on one of edges of the two-dimensional topological insulator, a gap is opened in the corresponding gapless edge states but another pair of gapless edge states with opposite spin are still protected by the time-reversal symmetry. So the conductance plateaus with the half-integer values e^2/h can be obtained in the gap induced by magnetic impurities, which means that the pure spin current can be induced in the sample. We also find that the pure spin current is insensitive to weak disorder. The mechanism to generate pure spin currents is generalized for two-dimensional topological insulators.

PACS numbers: 75.76.+j; 72.80.Vp; 03.65.Vf

Since graphene, a single-layer honeycomb lattice of carbon atoms, has been prepared laboratorially by Novoselov et al.,[1] it has attracted considerable attentions due to its novel properties in condensed matter physics and potential applications in devices. [2–10] Graphene is the first independent two-dimensional (2D) crystal that has been experimentally achieved, which leads to new interests in 2D systems. For example, the Kane-Mele model, a quantum spin Hall effect (QSHE) was first proposed in graphene with spin-orbital coupling, which is the first example of topological insulator.[11, 12] Topological insulators are time-reversal symmetric systems whose intrinsic spin-orbit coupling (SOC) opens a bulk gap while generating the Kramers doublet of edge states owing to the nontrivial Z_2 invariants of the occupied bands. The edge states force electrons with opposite spin to flow in opposite directions along the edges of the sample, which lead to quantized spin Hall conductance. However, the intrinsic SOC in realistic graphene is quite weak and the gap opening was small, so the QSHE in graphene is difficult to be observed.[13] Nevertheless, recently a monolayer honeycomb lattice of silicon called silicene has been synthesized and attracts much attention.[14–17] Silicene has a relatively large intrinsic spin-orbit gap of 1.55meV , as makes experimentally accessible the Kane-Mele type QSHE.[16]

The development of the topological insulator opens a new and powerful way for the spintronic applications due to its spin-dependent edge states. How to generate pure spin currents in low-dimensional systems is the main challenge in the field of spintronics. The aim of this work is to propose a method for generating a pure spin current in a 2DTI. In this Letter, as a concrete example, we theoretically study the electron transport in Kane-Mele model with magnetic doping at one edge, as shown in Fig. 1. Most of the results are also applicable to general 2DTIs. Before presenting our detailed calculations, we first analyze why pure spin current can be gen-

erated in the present device. The intrinsic SOC which originates from intra-atomic SOC, converts the sample into a topological insulator with a QSHE.[11] The gapless edge states are protected by time-reversal symmetry and is thus robust to non-magnetic impurities that do not break this symmetry. But a pair of edge states are destroyed when magnetic impurities exist on this corresponding edge (see Fig. 1). Because another pair of edge states, with opposite spins containing opposite propagation directions, are still protected by time-reversal symmetry, we can observe a pure spin current in the sample, which is confirmed by our following calculations.

In the tight-binding representation, we consider the Kane-Mele Hamiltonian defined on a honeycomb lattice:[11, 12]

$$\begin{aligned} H = & t \sum_{\langle ij \rangle, \sigma} c_{i\sigma}^\dagger c_{j\sigma} + i\lambda \sum_{\langle\langle ij \rangle\rangle, \sigma} \nu_{ij} c_{i\sigma}^\dagger s_z c_{j\sigma} \\ & + i\alpha \sum_{\langle ij \rangle, \sigma} c_{i\sigma}^\dagger (\mathbf{s} \times \mathbf{d}_{ij})_z c_{j\sigma} + \lambda_\nu \sum_{i, \sigma} \xi_i c_{i\sigma}^\dagger c_{i\sigma}. \quad (1) \end{aligned}$$

The symbols $\langle ij \rangle$ and $\langle\langle ij \rangle\rangle$ denote the nearest and the next-nearest neighbors, respectively, and $\sigma = \uparrow, \downarrow$ (or ± 1) denotes spin index. The first term is the nearest-neighbor hopping. The second term describes the intrinsic SOC. Here the site-dependent Haldane phase factor[11] ν_{ij} is defined as $\nu_{ij} = (\mathbf{d}_1 \times \mathbf{d}_2)/|\mathbf{d}_1 \times \mathbf{d}_2| = \pm 1$, where \mathbf{d}_i denotes the vector from one atom to one of its nearest neighbors. s_z is a Pauli matrix describing the electron's spin. The third term is a nearest neighbor Rashba SOC term, which can be produced by applying an electric field perpendicular to the sheet. The fourth term is a staggered sublattice potential ($\xi_i = \pm 1$). It is interesting to notice that, Eq. (1) is almost applicable to silicene except for the Rashba SOC term, which is present between the next-nearest neighbors in silicene but between the nearest neighbors in our model. The focus of this work is the introduction of magnetic impurities (red square dots

in Fig. 1) on the uppermost zigzag chain of the sample ($n = 1$),

$$\sum_{i \in \{n=1\}, \sigma} \sigma M c_{i\sigma}^\dagger c_{i\sigma} \quad (2)$$

where M is the strength of exchange interaction induced by the magnetic impurities. This term breaks the local time reversal symmetry on the upper edge.

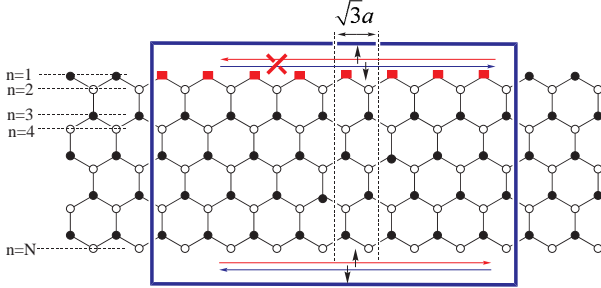


FIG. 1: (Color online) Schematic diagram of a zigzag honeycomb lattice nanoribbon with magnetic impurities (red square dots) on the upper edge. Its unit cell is marked by the dashed lines. The red and blue arrows at the edges denote propagation directions of the opposite spins in the edge states.

In the following numerical calculations, we use the hopping energy t as the energy unit. The width N is chosen as $N = 50$ in all calculations and the nearest neighbor atom-atom distance is a . The strengths of the intrinsic SOC, the Rashba SOC and the staggered sublattice potential are $\lambda = 0.06t$, $\alpha = 0.05t$, and $\lambda_\nu = 0.1t$, respectively. These parameters define the system as a two-dimensional topological insulator.[11]

First, we investigate the energy subbands obtained by solving the lattice model in strip geometry, as shown in Fig. 2. In the pure case ($M = 0$, Fig. 2(a)), the edge states traverse the energy gap in pairs. The gapless edge states are robust against small non-magnetic perturbations since they are protected by time reversal symmetry.[11] However, in the presence of magnetic impurities ($M \neq 0$, Fig. 2(b)-(d)) at the upper edge, the corresponding pair of gapless edge states is destroyed and a gap can be opened due to the local time reversal symmetry breaking. Moreover, the magnitude of the gap opened by the magnetic impurities increases with enhanced M , and can reach $0.18eV$ for $M = 1.0t$. Another pair of gapless edge states, still protected by time reversal symmetry, persist on that edge without magnetic impurities. But the electron-hole symmetry is broken in the preserved gapless edge states, which cross at $ka = \pi$ even for a very small value of M .

Next, we examine the influence of the magnetic impurities on the conductance of the system, as shown in Fig. 3. The two-terminal conductance of the system can be calculated by the nonequilibrium

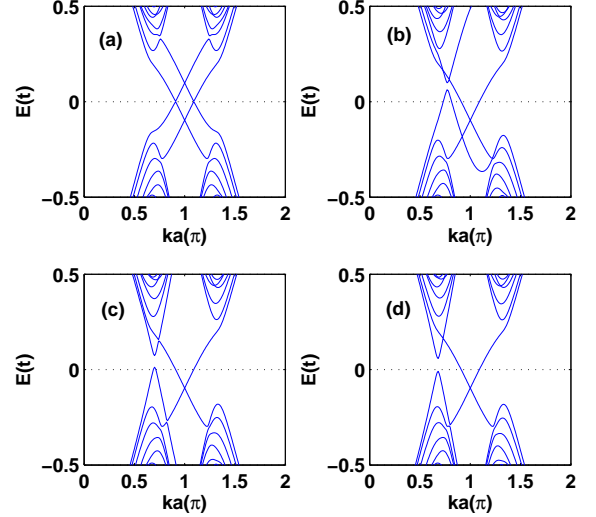


FIG. 2: (Color online) Calculated energy bands in the zigzag honeycomb lattice nanoribbon in the presence of the intrinsic spin-orbit coupling and the Rashba spin-orbit coupling for $M = 0$ (a), $M = 0.4t$ (b), $M = 0.8t$ (c), and $M = 1.0t$ (d).

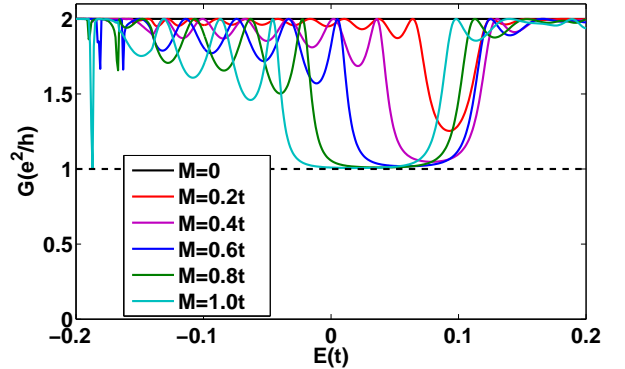


FIG. 3: (color online) The conductance G vs E for different M .

Green's function method and the Landauer-Büttiker formula $G(E) = \frac{e^2}{h} \text{Tr}[\Gamma_L(E)\mathbf{G}^r(E)\Gamma_R(E)\mathbf{G}^a(E)]$, where $\Gamma_p(E) = i[\Sigma_p^r(E) - \Sigma_p^a(E)]$ is the line-width function and $\mathbf{G}^r(E) = [\mathbf{G}^a(E)]^\dagger = 1/[\mathbf{E} - \mathbf{H}_{cen} - \Sigma_L^r - \Sigma_R^r]$ is the retarded Green function with the Hamiltonian in the center region \mathbf{H}_{cen} .[18] The self-energy Σ_p^r due to the semi-infinite lead- p can be calculated numerically.[19] In the case of $M = 0$, the quantized conductance plateau appears, with the plateau value $2e^2/h$ coming from the contributions of two pairs of the gapless edge states. For greater values of M , the conductance plateau $2e^2/h$ is suppressed and evolves into a conductance plateau e^2/h in the energy gap opened by the magnetic impurities. The conductance plateau e^2/h is only contributed from the gapless edge states at the lower edge without mag-

netic impurities, which can be seen from Fig. 4. Without magnetic impurities ($M = 0$), there are two pairs of perfect edge states with opposite spins at two edges of the sample, so the currents through the sample is spin unpolarized. However, when the gapless edge states at the upper edge are destroyed by magnetic impurities ($M \neq 0$), the spin-velocity locked channels persist only at the lower edge of the sample. Therefore, the current in the sample consists of the opposite spins moving in opposite directions that is called pure spin current, which is just the aim of the present work. For a definite arrangement of bias voltage, there remains only, say, right going channels with spin up working. Moreover, the pure spin current in the sample is really invariant under time reversal.

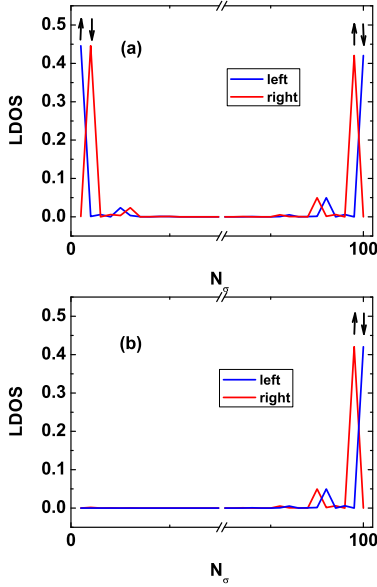


FIG. 4: (Color online) Spin-resolved local density of states (LDOS) along the width of sample for (a) $M = 0$ and (b) $M = 1.0$. The energy is chosen $E = 0.02t$ in the simulation. $N_\sigma = 2n - 1$ and $N_\sigma = 2n$ correspond to spin-up and spin-down LDOS, respectively, where $N_\sigma = 1, 2, \dots, 2N$. The black up and down arrows denote spin up and spin down. The blue and red curves denote left and right propagation direction

To test the above arguments in a more direct way, we also studied the spin-resolved conductance and spin polarization when the magnetic impurities exist on the upper edge of the sample. For the sake of simplicity, we assume that in the leads, the staggered sublattice potential, the intrinsic and Rashba SOC do not exist, i.e., the Hamiltonian of lead- p is simply

$$H_p = t \sum_{\langle ij \rangle, \sigma} c_{i\sigma}^\dagger c_{j\sigma}. \quad (3)$$

The spin-resolved conductance matrix can be written as

$$G = \begin{pmatrix} G_{\uparrow\uparrow} & G_{\uparrow\downarrow} \\ G_{\downarrow\uparrow} & G_{\downarrow\downarrow} \end{pmatrix}, \quad (4)$$

which can also be calculated by generalized Landauer formula for spin transport. The conductance $G_{\uparrow\uparrow}$ and $G_{\uparrow\downarrow}$ can be obtained when we assume that only spin-up electrons are injected from the left lead into the sample and collected in the right lead. We can also calculate $G_{\downarrow\uparrow}$ and $G_{\downarrow\downarrow}$ in the same way by assuming only spin-down electrons are injected from the left lead. The total conductance G and the spin polarization P in lead- R can be respectively defined as[20, 21]

$$G = G_{\uparrow\uparrow} + G_{\downarrow\uparrow} + G_{\uparrow\downarrow} + G_{\downarrow\downarrow} \quad (5)$$

and

$$P = \frac{G_{\uparrow\uparrow} + G_{\downarrow\uparrow} - G_{\uparrow\downarrow} - G_{\downarrow\downarrow}}{G_{\uparrow\uparrow} + G_{\downarrow\uparrow} + G_{\uparrow\downarrow} + G_{\downarrow\downarrow}}. \quad (6)$$

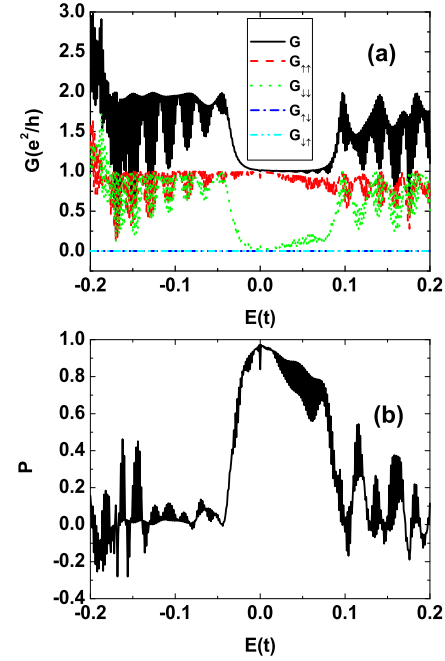


FIG. 5: (Color online) Spin-resolved conductance (a) and spin polarization (b) vs E for $M = 1.0$. The parameters $\lambda = 0$, $\alpha = 0$, and $\lambda_\nu = 0$ are chosen in leads

Fig. 5 (a) and (b) show the spin-resolved conductance G and spin polarization P versus the energy E for $M = 1$. In Fig. 5 (a), the total conductance manifests itself with the plateau value e^2/h due to the presence of the magnetic impurities on the upper edge of the central region. Due to the topological nature of the edge states, this

plateau is insensitive to the mismatch between the sample and the leads. We can also find that the spin-up and spin-down electrons are not mixed when they transport through the sample, i.e., $G_{\uparrow\downarrow} = G_{\downarrow\uparrow} = 0$. The spin polarization can almost reach 100% in the energy gap opened by the magnetic impurities [see Fig. 5 (b)] because the spin-up electron can fully transport through the sample while the spin-down electron can hardly transport through the sample in the gap [see Fig. 5 (a)]. Beyond the gap, due to the conduction band mismatch between the central region and the leads, there are resonant tunneling peaks in the conductance beyond the gap induced by the magnetic impurities, as shown in Fig. 3 and Fig. 5.

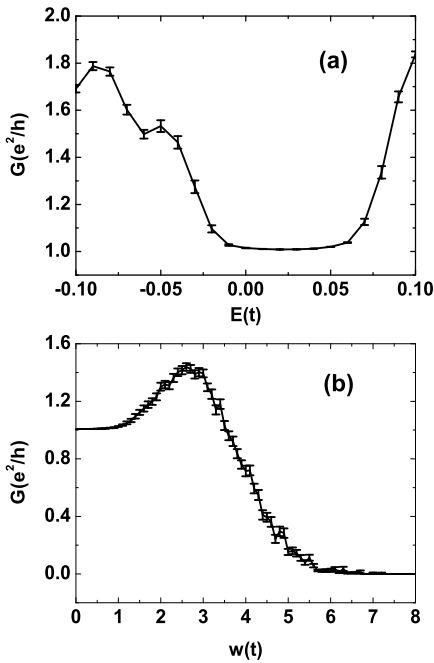


FIG. 6: The conductance G as a function of the energy E for the disorder strengths $w = 0.5t$ (a) and as a function of the disorder strengths w for the energy $E = 0.02t$ (b). The error bars show standard deviation of the conductance for 100 samples.

Finally, we examine the non-magnetic disorder effect on this spin-polarized conductance plateau e^2/h . Due to disorder, random on-site potential w_i is added for each site i in the central region, where w_i is uniformly distributed in the range $[-w/2, w/2]$ with the disorder strength w . Fig. 6 (a) and (b) show the conductance G versus the energy E at the disorder strength $w = 0.5t$ and G versus the disorder strength w at the energy $E = 0.02t$, respectively. The results show that the quantum plateau of e^2/h is very robust against non-magnetic disorder because of the topological origin of the edge states. The

quantum plateau maintains its quantized value very well even when w reaches $1.0t$. The robust and stable plateau of e^2/h means that the pure spin current of the system is insensitive to weak disorder and protected by time-reversal symmetry. In addition, even for a large disorder strength w (e.g., from $w = 1.0t$ to $w = 3.0t$), the conductance is increased rather than decreasing with the increasing disorder strength. This is because although the strong disorder weakens the edge states, it also result in the mobility of the energy band structure,[22] so the value of G increases in the range of $w = 1.0t$ to $w = 3.0t$. With further increasing of the disorder strength, the conductance gradually reduce to zero, the system eventually enters the insulating regime.

In summary, we predict a new mechanism to generate a pure spin current in a two-dimensional topological insulator. As the magnetic impurities exist on one edge of the sample, the corresponding gapless edge states is destroyed but another pair of gapless edge states with opposite spin are protected by time-reversal symmetry. So a pure spin current with the spin-up and spin-down carriers moving in opposite directions can be observed in the system. Moreover, the pure spin current has also been found to be robust against non-magnetic disorder. The mechanism to generate pure spin currents can be generalized for two-dimensional topological insulators, such as HgTe/CdTe quantum well and silicene nanoribbons.

This work was supported by National Natural Science Foundation of China (Grant Nos. 11047184, 11104059, No. 61176089) and Hebei province Natural Science Foundation of China (Grant No. A2011208010).

-
- * Electronic address: anxingtao@semi.ac.cn
- [1] K. S. Novoselov, A. K. Geim, S. V. Morozov, D. Jiang, Y. Zhang, S. V. Dubonos, I. V. Grigorieva, and A. A. Firsov, *Science* **306**, 666 (2004).
 - [2] A. K. Geim and K. S. Novoselov, *Nat. Mater.* **6**, 183 (2007).
 - [3] A. K. Geim, *Science* **324**, 1530 (2009).
 - [4] A. H. C. Neto, F. Guinea, N. M. R. Peres, K. S. Novoselov, and A. K. Geim, *Rev. Mod. Phys.* **81**, 109 (2009).
 - [5] C. W. J. Beenakker, *Rev. Mod. Phys.* **80**, 1337 (2008).
 - [6] D. S. L. Abergel, V. Apalkov, J. Berashevich, K. Ziegler, and T. Chakraborty, *Adv. Phys.* **59**, 261 (2010).
 - [7] S. D. Sarma, S. Adam, E. H. Hwang, and E. Rossi, *Rev. Mod. Phys.* **83**, 407 (2011).
 - [8] Q.-F. Sun and X. C. Xie, *Phys. Rev. Lett.* **104**, 066805 (2010).
 - [9] Y. Zhang, Y.-W. Tan, H. L. Stormer, and P. Kim, *Nature (London)* **438**, 201 (2005).
 - [10] J. R. Williams, L. Dicarlo, and C. M. Marcus, *Science* **317**, 638 (2007).
 - [11] C. L. Kane and E. J. Mele, *Phys. Rev. Lett.* **95**, 146802 (2005).
 - [12] C. L. Kane and E. J. Mele, *Phys. Rev. Lett.* **95**, 226801

- (2005).
- [13] Y. Yao, F. Ye, X.-L. Qi, S.-C. Zhang, and Z. Fang, Phys. Rev. B **75**, 041401(R) (2007).
 - [14] B. Lalmi, H. Oughaddou, H. Enriquez, A. Kara, S. Vizzini, B. Ealet, and B. Aufray, Appl. Phys. Lett. **97**, 223109 (2010).
 - [15] B. Feng, Z. Ding, S. Meng, Y. Yao, X. He, P. Cheng, L. Chen, and K. Wu, cond-mat/arXiv:1203.2745 (2012).
 - [16] C.-C. Liu, W. Feng, and Y. Yao, Phys. Rev. Lett. **107**, 076802 (2011).
 - [17] M. Ezawa, cond-mat/arXiv:1203.0705 (2012).
 - [18] W. Ren, Z. Qiao, J. Wang, Q.-F. Sun, and H. Guo, Phys. Rev. Lett. **97**, 066603 (2006).
 - [19] M. P. L. Sancho, J. M. L. Sancho, and J. Rubio, I. Phys. F: Met. Phys. **15**, 851 (1985).
 - [20] S. Bellucci and P. Onorato, Phys. Rev. B **77**, 075303 (2008).
 - [21] Y. Ming, J. Gong, and R. Q. Zhang, J. Appl. Phys. **110**, 093717 (2011).
 - [22] Y.-Y. Zhang, R.-L. Chu, F.-C. Zhang, and S.-Q. Shen, Phys. Rev. B **85**, 035107 (2012).